Dyes and Pigments 193 (2021) 109485

Contents lists available at ScienceDirect

Dyes and Pigments

journal homepage: www.elsevier.com/locate/dyepig

Phosphine-based push-pull AIE fluorophores: Synthesis, photophysical properties, and TD-DFT studies

Maxime Rémond [a], Pauline Colinet [a], Erwan Jeanneau [b], Tangui Le Bahers [a], Chantal Andraud [a], Yann Bretonnière [a,*]

[a] Université de Lyon, École Normale Supérieure de Lyon, Université Lyon 1, CNRS UMR 5182, Laboratoire de Chimie, 46 Allée D'Italie, 69364, Lyon, France
[b] Université de Lyon, Centre de Diffractométrie Henri Longchambon, Université Lyon I, 43 Boulevard Du 11 Novembre 1918, 69622, Villeurbanne, Cedex, France

ARTICLE INFO

Keywords:
Phosphine based dyes
Push-pull dyes
DFT
AIE
Large Stokes shift

ABSTRACT

Herein, we report the design and characterization of a novel series of four push-pull fluorophores using diphenylphosphino as an electron-donating terminal group (P-chromophores). The spectroscopic properties in solution, the aggregation-induced emission (AIE) properties, as well as the emission properties in the solid state were studied and compared with those of the diphenylamino-analogues (N-chromophores). Comparative analysis of the crystalline structures coupled with density functional theory calculations revealed that the diphenylphosphino group adopts a pyramidal geometry, whereas a trigonal planar configuration around the N-center is observed for the diphenylamino group. Consequently, the phosphorous lone pair is localized on the upper side of the average chromophore plan and considerable geometrical change of the P-center can occur between the ground state and the first excited state, explaining the much larger Stokes shift observed (10 000 cm^{-1}) for the P-chromophores compared to the N-analogues.

1. Introduction

Organic synthesis offers virtually endless possibilities to fine-tune the optical properties of organic fluorophores. To this end, the incorporation of heteroatoms into the chromophore π -backbone is an effective structure-modification strategy inducing significant electronic perturbations in the parent molecules and, usually, a large wavelength shift. While light main-group heteroatoms such as boron (B), nitrogen (N), or oxygen (O) have been extensively used[1–3], heavier second-row elements such as phosphorous (P) have been rather neglected, especially in small push-pull molecules. However, straightforward chemical transformations of the P-center through oxidation/reduction, complexation with metal ion or quaternarization provides numerous options to modulate the photophysical and electrochemical properties of π-electron frameworks in which the P-center is embedded or grafted. $\lambda^5\sigma^4$ (phosphorus oxide or sulfide) and $\lambda^4\sigma^4$ phosphorus groups (phosphonium cations) behave as strong electron-withdrawing groups [4–6] but has only seldom been used as such in simple combination with donor groups to construct dipolar rod-shaped [7–12] or three-dimensional star-shaped octupolar chromophores[10,12,13].

By contrast, $\lambda^5\sigma^4$ and $\lambda^4\sigma^4$ P-heterocyclic compounds, containing either a five-membered phosphole ring [14–23] or six-membered ring variants[24–37], showed great potential for the construction of interesting far-red emissive π-conjugated structures. The obtained cyclic-organophosphorous derivatives differ from their widely used sulphur or nitrogen analogues by a substantial bathochromic shift of absorption and emission up to the NIR[25,30,34]. This can be ascribed to the lower aromaticity bestowed by specific orbital interactions between the exocyclic σ*(P-R) or σ*(P═O) and π* (butadiene) orbitals, together with the pyramidal configuration of the phosphorus atom[14,17,18].

Besides phosphole derivatives, there are few examples of chromophores containing a $\lambda^3\sigma^3$ P-center in general and phosphine particularly. The lesser interest for P(III) can be explained by its sensitivity towards oxidation, particularly in solution, which limits synthetic yields, spectroscopic studies and final applications. However, P(III) to P(V) oxidation can be prevented by delocalization of the lone pair in a π-system. Thus, conjugated phosphines, such as triphenylphosphine or BINAP, are quite stable towards oxidation. Using this strategy, stable primary or tertiary phosphines linked to a BODIPY derivative were synthesized by Higham et al. for metal sensing[38,39]. However, this approach can be limited by potential fluorophore quenching due to a photoinduced

* Corresponding author.
E-mail address: yann.bretonniere@ens-lyon.fr (Y. Bretonnière).

https://doi.org/10.1016/j.dyepig.2021.109485
Received 24 February 2021; Received in revised form 17 May 2021; Accepted 17 May 2021
Available online 28 May 2021

electron transfer to the nearby phosphine[40,41]. Fluorescent $\lambda^3\sigma^3$ phosphines were nevertheless obtained by either including the phosphorus atom in a fused π system [42] or with three extended π-systems around the phosphorus atom[43]. It is also possible to use the electron donating capacities of phosphines to design intramolecular charge transfer dyes. For example, Madrigal et al. studied the absorption properties of quadripolar and octupolar triphenylamine and triphenylphosphine stilbene derivatives[44–46]. The absorption and non-linear optical properties of a dipolar dye containing a phosphine donor and a nitro acceptor, as well as a few donor/acceptor structures, based on an aryl phosphine coupled with a boron acceptor, were also investigated [47,48]. Finally, Baumgartner et al. studied 2,7-diketophosphepin as fluorescent π-conjugated building blocks[49]. Interestingly, some of those compounds showed solid-state emission, but quantum yields were not reported.

Hence, only a few examples of fluorescent phosphine derivatives have been studied, even fewer in a push-pull configuration, and none of them emit in the biological window (650 nm–1000 nm) for imaging applications. It appears that more studies of these derivatives are called for. Indeed, thanks to the intramolecular charge transfer from the donor to the acceptor end, these chromophores have unique optical properties such as a large Stokes shift that any variation of the donor or the acceptor end will modify.

Herein, we used P-$\lambda^3\sigma^3$ triphenylphosphine as the donor group in a series of small push-pull fluorophores (**P1**–**P4**, Fig. 1) incorporating various potent electron acceptor groups **1**–**4**. The optical properties in solution but also in the solid state were measured and compared with those of the triphenylamine analogues (**N1**–**N4**) that we reported previously[50–52]. The influence of the donor atom on the optical properties was rationalized by comparison with the X-ray diffraction structures and by theoretical calculations. In particular, we showed that conformational changes around the P-atom between the ground state and the first excited state led to higher fluorescence turn-on coefficients upon aggregation (170-fold increase emission for **P2**) than their amine analogues, as well as a drastically increased Stokes shift (up to 10 000 cm^{-1} on average).

2. Materials and methods

2.1. General

Commercially available materials were used as received. Analytical thin-layer chromatography (TLC) was carried out on Merck 60 F254 precoated silica gel plate (0.2 mm thickness). Visualization was performed using a UV lamp (254 nm or 365 nm). Anhydrous THF was distilled over sodium and benzophenone. Microwave synthesis were conducted in 10 mL sealed tube on a Biotage Initiator 2.5 single-mode reactor using external IR temperature control. Column chromatography was performed on Merck silica gel Si-60 (40–63 μm). NMR spectra were recorded at ambient temperature on a standard spectrometer operating at 400 MHz or 300 MHz for ^{1}H NMR, 125 MHz or 101 MHz for ^{13}C NMR and 202 MHz or 162 MHz for ^{31}P NMR. Chemical shifts are given in parts per million (ppm) and are reported relative to tetramethylsilane (^{1}H, ^{13}C) using the residual solvent peaks as internal standard.

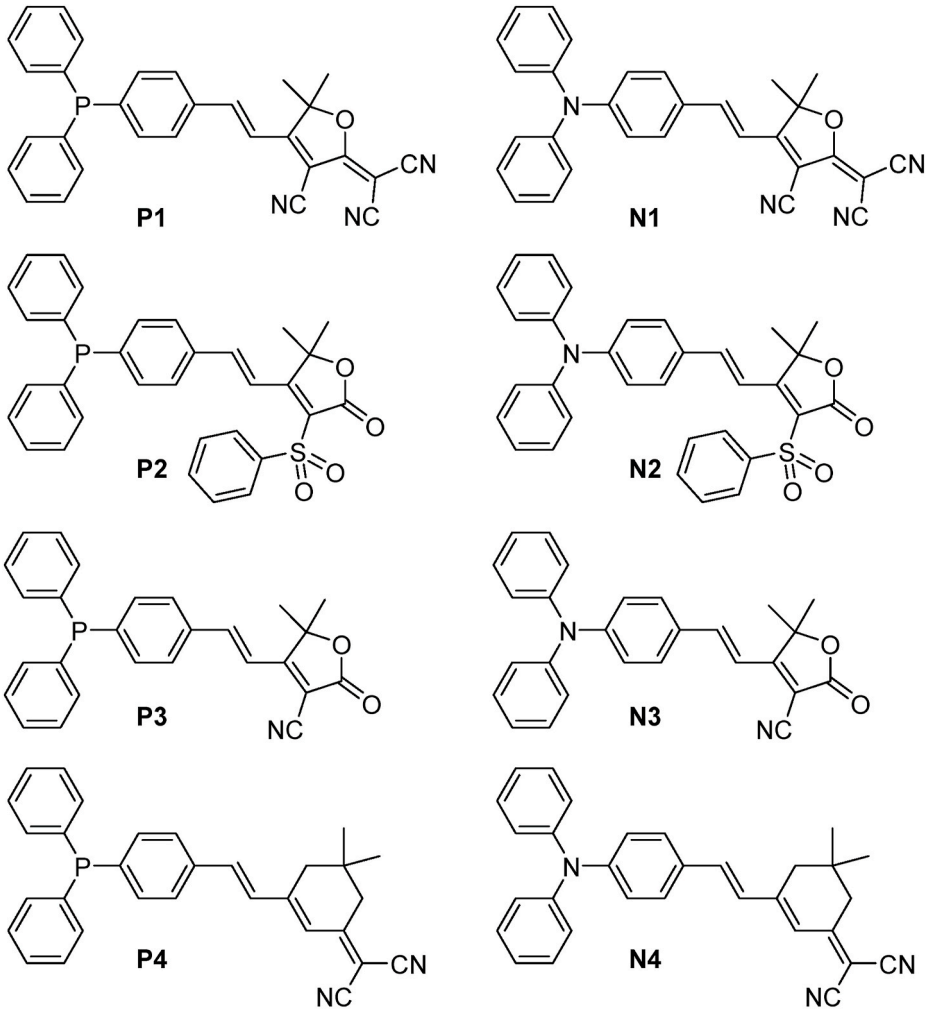

Fig. 1. Structures of the P-λ3σ3 chromophores **P1**–**P4** and nitrogen analogues **N1**–**N4**.

^{1}H NMR splitting patterns are designated as singlet (s), doublet (d), triplet (t), quartet (q), dd (doublet of doublets), q (quadruplet), quint (quintuplet) or m (multiplet). Low resolution mass spectra were measured at 298 K by direct injection of dilute sample into the mass analyzer of an Agilent Technologies 1260 Infinity LC-MS instrument. High-resolution mass spectrometry (HRMS) measurements were performed by ESI-QTOF mass spectrometry (Bruker Daltonics MicroTOF-Q II) at the *Centre Commun de Spectrométrie de Masse* (UCBL, Villeurbanne, France). Compound **1**[53], **2** and **3**[52], and **4** [50] were obtained according to reported procedure.

2.2. Synthetic procedures and characterization data

2.2.1. 2-(4-Bromophenyl)-1,3-dioxolane [54–56]

4-Bromobenzaldehyde (2 g, 10.8 mmol) and p-toluenesulfonic acid (0.2 g, 1 mmol) were dissolved in toluene (50 mL), and an excess of ethylene glycol (2 mL, 35 mmol) was added. The mixture was then heated to reflux overnight with azeotropic removal of water by a Dean–Stark trap. After cooling, the solution was washed three times with saturated aqueous Na_2CO_3, dried over Na_2SO_4, filtrated and concentrated. Purification by column chromatography on silica eluting with CH_2Cl_2/petroleum ether (v/v 1:1) gave a white solid (2.3 g, 93%). ^{1}H NMR (300 MHz, $CDCl_3$, δ/ppm) 7.51 (d, J = 8.4 Hz, 2H), 7.35 (d, J = 8.4 Hz, 2H), 5.77 (s, 1H), 4.15–3.98 (m, 4H); ^{13}C{^{1}H}-NMR (100 MHz, $CDCl_3$, δ/ppm) 137.2, 131.7, 128.3, 123.4, 103.2, 65.5; HR-MS (ESI-QTOF, pos) m/z calcd for $C_9H_9BrO_2$: 227.9780 $[M]^+$, found: 227.9751.

2.2.2. 2-(Diphenylphosphino)-1,3-dioxolane [57–59]

2-(4-Bromophenyl)-1,3-dioxolane (2.2 g, 9.6 mmol) was dissolved in anhydrous THF under argon and cooled to −78 °C. *n*BuLi (2.5 M in hexanes, 4.25 mL, 10.6 mmol) was added dropwise and the mixture was stirred for 1 h at −78 °C. Chlorodiphenylphosphine (2.2 g, 10 mmol) in anhydrous THF (5 mL) was then added dropwise. The temperature was let heat up to RT and the solution was stirred overnight. The reaction was quenched with saturated NH_4Cl (4 mL) and the layers were separated. The organic layer was washed with water and brine, dried over Na_2SO_4, filtered and concentrated under vacuum to give a yellow oil. The product was purified over silica gel chromatography eluting with CH_2Cl_2 and a white solid was obtained (1.5 g, 47%). *An attempt to recrystallize the product in EtOH only led to partial oxidation of the phosphine*. ^{1}H NMR (300 MHz, $CDCl_3$, δ/ppm) 7.48–7.41 (m, 2H), 7.39–7.26 (m, 12H), 5.80 (s, 1H), 4.15–4.00 (m, 4H); ^{13}C{^{1}H} NMR (100 MHz, $CDCl_3$, δ/ppm) 138.7 (d, $J_{p\text{-}c}$ = 11.5 Hz), 138.5, 137.1 (d, $J_{P\text{-}C}$ = 10.7 Hz), 133.9 (d, $J_{P\text{-}C}$ = 19.5 Hz), 128.9, 128.7 (d, $J_{P\text{-}C}$ = 7.0 Hz), 126.7 (d, $J_{P\text{-}C}$ = 7.0 Hz), 103.6, 65.5; ^{31}P{^{1}H}-NMR (162 MHz, $CDCl_3$, δ/ppm) −5.6; HR-MS (ESI-QTOF, pos) m/z calcd for $C_{21}H_{20}O_2P$: 335.1195 $[M+H]^+$, found: 335.1201.

2.2.3. 4-(Diphenylphosphino)benzaldehyde P [57–59]

2-(Diphenylphosphino)-1,3-dioxolane (1.5 g, 4.5 mmol) was dissolved in a toluene (10 mL)/water (1 mL) mixture before addition of p-toluenesulfonic acid (20 mg, 0.1 mmol). The mixture was refluxed and the reaction monitored by TLC. After completion, the mixture was let cool down to RT and more water (5 mL) was added. The mixture was extracted 3 times with ethyl acetate. The combined organic phases were washed 3 times with saturated Na_2CO_3, dried over Na_2SO_4, filtered and concentrated to give a yellow oil. The crude was purified over silica gel chromatography with CH_2Cl_2 as eluent to obtain P as a white solid (1.05 g, 81%). ^{1}H NMR (300 MHz, $CDCl_3$, δ/ppm) 10.0 (s, 1H), 7.85–7.77 (m, 2H), 7.46–7.29 (m, 12H); ^{13}C{^{1}H}-NMR (100 MHz, $CDCl_3$, δ/ppm) 192.1, 146.6 (d, $J_{P\text{-}C}$ = 15.6 Hz), 136.1, 135.9 (d, $J_{P\text{-}C}$ = 10.5 Hz), 134.2 (d, $J_{P\text{-}C}$ = 20.2 Hz), 133.7 (d, $J_{P\text{-}C}$ = 18.5 Hz), 129.5, 128.9 (d, $J_{P\text{-}C}$ = 7.4 Hz); ^{31}P{^{1}H}-NMR (162 MHz, $CDCl_3$, δ/ppm) −4.3; HR-MS (ESI-QTOF, pos) m/z calcd for $C_{19}H_{16}OP$: 291.0933 $[M+H]^+$, found: 291.0926.

2.2.4. Synthesis of compounds P1–P4

In a 10 mL microwave tube, **P** (200 mg, 0.69 mmol) and the corresponding acceptor group (0.65 mmol) were suspended in absolute ethanol (4 mL). One drop of piperidine was added before sealing of the microwave tube. The reaction was heated to 100 °C by microwave irradiation during 30 min. After cooling down to RT, the precipitated dye was filtered and washed with cold ethanol. The dyes were purified by column chromatography over silica gel using the eluent indicated.

2.2.5. P1

From **P** and **1** (130 mg). Eluent: CH_2Cl_2. Red solid (200 mg, 65%). ^{1}H NMR (400 MHz, CD_2Cl_2, δ/ppm) 7.66–7.59 (m, 3H), 7.42–7.32 (m, 11H), 7.08 (d, J = 16.5 Hz, 2H), 1.78 (s, 6H); ^{13}C{^{1}H}-NMR (125 MHz, CD_2Cl_2, δ/ppm) 175.8, 174.3, 147.0, 145.0 (d, $J_{P\text{-}C}$ = 15.4 Hz), 136.5 (d, $J_{P\text{-}C}$ = 11.1 Hz, 2C), 134.4 (d, $J_{P\text{-}C}$ = 20.2 Hz), 134.3 (d, $J_{P\text{-}C}$ = 18.3 Hz), 129.7 (2C), 129.2 (d, $J_{P\text{-}C}$ = 7.3 Hz), 129.0 (d, $J_{P\text{-}C}$ = 6.2 Hz), 115.9, 112.1, 111.5, 110.6, 100.8, 98.4, 26.6; ^{31}P{^{1}H}-NMR (202 MHz, CD_2Cl_2, δ/ppm) −4.12; HR-MS (ESI-QTOF, pos) m/z calcd for $C_{30}H_{23}N_3OP$: 472.1573 $[M+H]^+$, found: 472.1558.

2.2.6. P2

From **P** and **2** (173 mg). Eluent: CH_2Cl_2/petroleum ether (v/v 1:1) to CH_2Cl_2. Yellow solid (250 mg, 71%). ^{1}H NMR (400 MHz, CD_2Cl_2, δ/ppm) 8.32 (d, J = 16.9 Hz, 1H), 8.08–8.03 (m, 2H), 7.70–7.62 (m, 3H), 7.59–7.54 (m, 2H), 7.41–7.33 (m, 12H), 7.26 (d, J = 16.9 Hz, 1H), 1.70 (s, 6H); ^{13}C{^{1}H}-NMR (125 MHz, CD_2Cl_2, δ/ppm) 171.1, 165.0, 144.4, 142.9 (d, $J_{P\text{-}C}$ = 14.3 Hz), 140.2, 136.9 (d, $J_{P\text{-}C}$ = 11.3 Hz), 135.5, 134.6, 134.4 (d, $J_{P\text{-}C}$ = 18.7 Hz), 134.3 (d, $J_{P\text{-}C}$ = 20.1 Hz), 129.6, 129.5, 129.1 (d, $J_{P\text{-}C}$ = 7.2 Hz), 128.9, 128.7 (d, $J_{P\text{-}C}$ = 6.4 Hz), 124.4, 116.8, 85.7, 27.4; ^{31}P{^{1}H}-NMR (202 MHz, CD_2Cl_2, δ/ppm) −4.86; HR-MS (ESI-QTOF, pos) m/z calcd for $C_{32}H_{28}O_4PS$: 539.1440 $[M+H]^+$, found: 539.1425.

2.2.7. P3

From **P** and **3** (100 mg). Eluent: CH_2Cl_2. Red solid (140 mg, 51%). ^{1}H NMR (400 MHz, CD_2Cl_2, δ/ppm) 7.68 (d, J = 16.5 Hz, 1H), 7.62–7.57 (m, 2H), 7.42–7.30 (m, 12H), 6.95 (d, J = 16.4 Hz, 1H), 1.67 (s, 6H); ^{13}C{^{1}H}-NMR (125 MHz, CD_2Cl_2, δ/ppm) 176.4, 166.3, 145.3, 143.4 (d, $J_{P\text{-}C}$ = 14.9 Hz), 136.7 (d, $J_{P\text{-}C}$ = 11.1 Hz), 134.7, 134.3 (d, $J_{P\text{-}C}$ = 20.2 Hz), 134.3 (d, $J_{P\text{-}C}$ = 18.8 Hz), 129.6, 129.1 (d, $J_{P\text{-}C}$ = 7.2 Hz), 128.6 (d, $J_{P\text{-}C}$ = 6.2 Hz), 116.0, 112.5, 99.6, 87.4, 26.1; ^{31}P{^{1}H}-NMR (202 MHz, CD_2Cl_2, δ/ppm) −4.67; HR-MS (ESI-QTOF, pos) m/z calcd for $C_{27}H_{23}NO_2P$: 424.1461 $[M+H]^+$, found: 424.1448.

2.2.8. P4

From **P** and **4** (121 mg). Eluent: CH_2Cl_2. Red solid (70 mg, 23%).^{1}H NMR (400 MHz, CD_2Cl_2, δ/ppm) 7.51–7.47 (m, 2H), 7.40–7.28 (m, 12H), 7.07 (s, 2H), 6.85 (s, 1H), 2.61 (s, 2H), 1.48 (s, 2H), 1.07 (s, 6H); ^{13}C{^{1}H}-NMR (125 MHz, CD_2Cl_2, δ/ppm) 169.7, 154.2, 140.2 (d, $J_{P\text{-}C}$ = 13.3 Hz), 137.2 (d, $J_{P\text{-}C}$ = 11.3 Hz), 136.6, 136.5, 134.32 (d, $J_{P\text{-}C}$ = 18.4 Hz), 134.2 (d, $J_{P\text{-}C}$ = 19.8 Hz), 130.2, 129.4, 129.0 (d, $J_{P\text{-}C}$ = 7.1 Hz), 127.8 (d, $J_{P\text{-}C}$ = 6.6 Hz), 124.3, 113.9, 113.2, 79.3, 43.3, 39.5, 32.3, 28.1; ^{31}P{^{1}H}-NMR (202 MHz, CD_2Cl_2, δ/ppm) −5.29; HR-MS (ESI-QTOF, pos) m/z calcd for $C_{31}H_{28}N_2P$: 459.1985 $[M+H]^+$, found: 459.1975.

2.3. Spectroscopy

Absorption spectra were recorded on a JASCO V670 spectrophotometer. Excitation and fluorescence emission spectra were recorded using a Horiba-Jobin Yvon Fluorolog-3 spectrofluorimeter equipped with a Hamamatsu R928 or water-cooled R2658 photomultiplier tubes. Spectra were corrected for the intensity variations of both the excitation light source (lamp and grating) and the emission spectral response (detector and grating). All solvents were of spectrophotometric grade. Solid state measurements were performed using a calibrated integrating

sphere (model F-3018 from Horiba Jobin Yvon) collecting the full emission (2π steradians covered with spectralon®), and quantum yields were measured as described previously[53].

Absorption and fluorescence spectra in acetone and in acetone/water mixtures were measured for 10 μM solutions. Suspensions were made directly in the quartz fluorescence cells. Water and acetone were mixed in the cell in the proportion of the given water fraction (*f*w) to give a final volume of 2.5 mL 25 μL of stock dye solution (1 mM) in acetone were then quickly injected into the solvent mixture. The mixture was then shaken several times by hand to obtain the final suspension with a 10 μM dye concentration. α values were calculated by dividing the emission in acetone/water 10:90 mixture by the emission in acetone solution. Solvatochromism was measured on 8 μM (**P1**) and 4 μM (**P2**–**P4**) solutions of the dyes in toluene, CH_2Cl_2 or acetone.

2.3.1. Crystallography

Single crystals of **P1** suitable for X-ray diffraction were grown by slow diffusion of a non-solvent (EtOH) in a concentrated solution of dye ($CHCl_3$) at room temperature. CCDC 1563373 contains the supplementary crystallographic data for this paper. These data can be obtained free of charge from The Cambridge Crystallographic Data Centre via www.ccdc.cam.ac.uk/data_request/cif.

2.3.2. Computational details

All calculations were performed using Gaussian package[60]. At the ground state, the structure of all the compounds was optimized at the DFT/6-31G(d) level of theory using the M06-2X hybrid functional[61]. Bulk solvent effects (acetone) were considered using a continuum solvation model (C-PCM)[62]. For each compound, 10 vertical excitation energies and the associated excited state densities of interest were computed at the TD-DFT level with the same basis set and with the M06-2X functional. The charge transfers transitions were characterized thanks to the $D_{C,T}$ index developed by Le Bahers et al. [63] using the cubegen utility provided by the Gaussian package.

3. Results and discussion

3.1. Synthesis

Synthesis of compounds **P1**–**P4** from 4-bromobenzaldehyde is depicted in Scheme 1. First, the aldehyde function was protected by formation of an acetal with ethylene glycol[54–56]. Then, the P-center was formed by a lithium-halogen exchange using *n*BuLi at −78 °C followed by nucleophilic substitution on chlorodiphenylphosphine. Finally, deprotection in acidic conditions gave 4-(diphenylphosphino) benzaldehyde **P**[57–59]. Note that, in our hands, this four steps methodology offered a much better overall yield of 4-(diphenylphosphino) benzaldehyde (35%) than direct palladium catalyzed phosphination of 4-bromobenzaldehyde using triphenylphosphine[64]. Compounds **P1**–**P4** were obtained in moderate to good yield (23 %–71%) by a Knoevenagel reaction with the active exocyclic methyl group of the corresponding electron-acceptors derivatives **1**–**4** [52] in ethanol using a catalytic amount of piperidine. The later step was performed under microwave irradiation, giving better yields than traditional heating.

The stability of the powder dyes to oxidation was verified by ^{1}H and ^{31}P NMR. After two years of storage at room temperature (15–30 °C) under air, the NMR of the redissolved powder showed no P(V) peak in ^{31}P NMR, nor any change of the protons' chemical shift. On the other hand, colorless solutions of **P2** or **P3** in acetone turned slightly yellow after one week.

3.2. Spectroscopic properties in solution

The optical properties of the dyes were studied in dilute acetone solutions. Spectra are shown in Fig. 2 and the optical properties are summarized in Table 1. The broad absorption of the dyes in the UV or visible range showed typical charge transfer transitions. For a given acceptor group, the absorption maxima were considerably blue-shifted for the P-dye compared to the amine dye. Whereas the absorption maxima of **N1**–**N4** were located between 460 nm and 540 nm, the absorption maxima of **P1**–**P4** ranged between 370 nm and 420 nm, with only **P1** in the visible range. This blue-shift, of 5000 cm^{-1} on average,

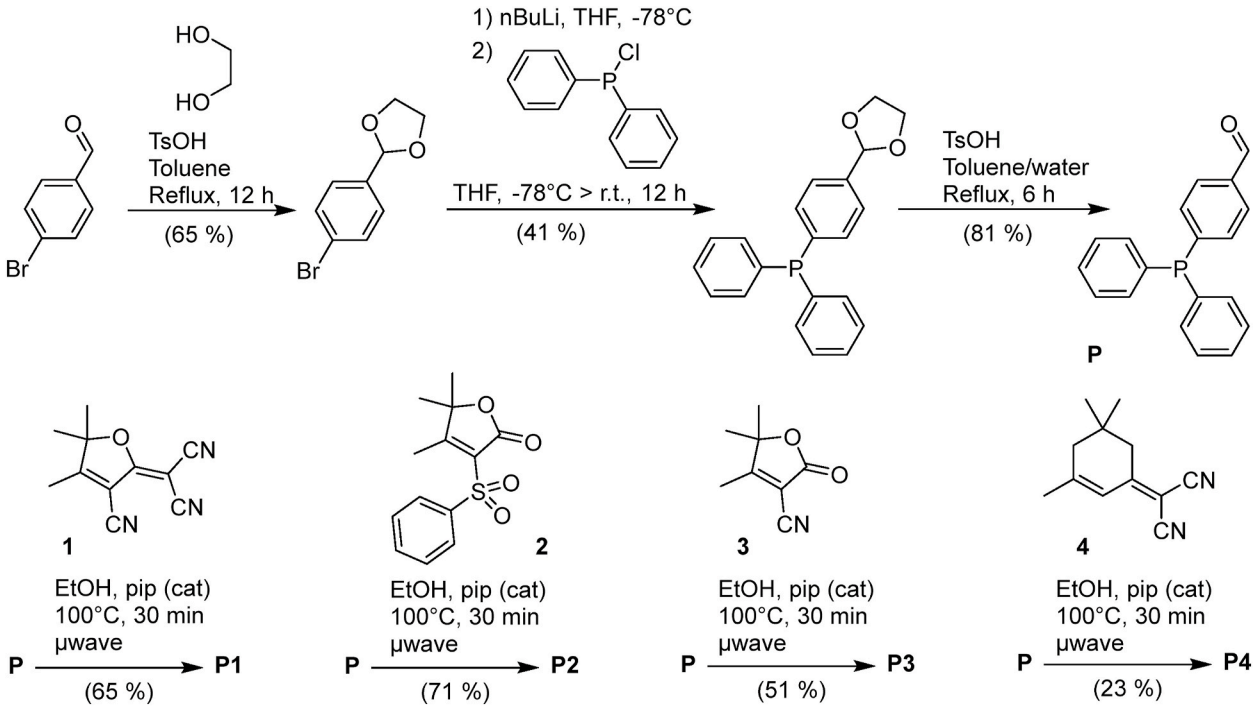

Scheme 1. Synthetic route to the target compounds **P1**–**P4**.

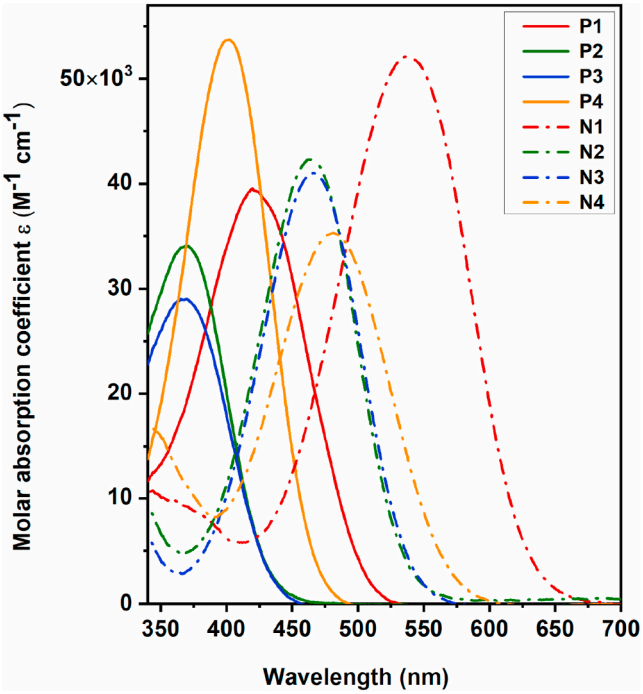

Fig. 2. Absorption spectra of **P1**–**P4** (plain lines) and **N1**–**N4** (dotted lines) in dilute solution in acetone.

was likely due to the lower donating capacity of phosphorus compared to nitrogen caused by the tetrahedral geometry of the former[14]. As anticipated, for a given donor group, increasing the strength of the electron accepting part led to an increase in the charge transfer, visible by the red-shift of the absorption. Finally, molar absorption coefficients ε were in the range of 30 000 to 50 000 $M^{-1}cm^{-1}$, which is very similar to what we previously reported for such small charge-transfer chromophores[51,52]. Note that for both P- and N- compounds the donor group does not seem to have a strong influence on the molar absorption coefficients values. A small solvatochromism is observed in absorption for all the dyes (Fig. SI 1 to SI 4, Table SI 1), and is higher for P-dyes compared to N-dyes. The highest effect is observed for **P2** with a 1446 cm^{-1} difference between the maximum in acetone and in dichloromethane.

In a dilute solution at room temperature, N-based chromophores **N1**–**N4** showed a moderate emission intensity that is strongly dependent on the solvent with a large red-shift, along with decrease in the quantum yield emission when the solvent polarity is increased[52]. A measurable emission was still obtained in polar acetone. On the contrary, P-based chromophores **P1**–**P3** were not emissive in any solvent. Only **P4** showed a weak orange fluorescence (centered at 600 nm) in toluene (Φ not measured, Fig. SI 5).

3.3. Spectroscopic properties in the solid-state

3.3.1. Aggregation-induced emission (AIE) properties

Interestingly, things considerably changed when studying the optical properties in the solid state. We have previously shown that the N-chromophores exhibited aggregation induced emission properties (AIE): the corresponding data are presented in Table 1 [51,52]. Nano-precipitation experiments were therefore performed to access the eventual AIE properties of the P-based chromophores. Absorption and emission spectra were recorded from different acetone/water mixtures of **P2** (10 μM) with increased volume fractions of water (f_w). As shown in Fig. SI 6, increasing the water fraction of the acetone/water mixtures above a critical water fraction ($f_w > 0.65$ here) resulted in the appearance of an orange fluorescence ($\lambda_{em} = 630$ nm) as well as a severe broadening of the absorption spectra, which is characteristic of AIE effect. A 170-fold increase of α_{AIE} (defined as the ratio in the fluorescence intensity between the aggregate and the solution in pure acetone, $f_w = 0$) was attained for $f_w = 0.9$. This is 17-fold more than for **N2** in the same conditions.

The other P-based chromophores **P1**, **P3** and **P4** also showed similar AIE properties in the orange to far-red region, and only the data for an acetone/water ratio $f_w = 0.9$ are given in Table 1 and Fig. 3. The α_{AIE} observed for the P-dyes are 7- to 70-folds higher than for the corresponding N-dyes. As observed for the dilute solution, the absorption spectra of the P-chromophores aggregates were strongly blue-shifted compared to their N analogues (around 5000 cm^{-1}). Hypochromic shifts were also observed in emission, albeit much less pronounced (around 1000 cm^{-1}). Indeed, the emission maxima obtained for the P-dyes ranged from 635 to 705 nm (against 655–750 nm for the N-dyes). Note the particularly long emission wavelength for compound **P1** (705 nm), which is particularly interesting for the design of turn-on probe for analytical or biological applications and is remarkable for a fluorophore with such a small molecular weight. This is the consequence of a considerably larger Stokes shift for the four P-based dye aggregates (9000-11000 cm^{-1}) than for their N-based analogues (5000-6000 cm^{-1}). This can be attributed to consequent geometrical changes between the ground state and the first excited state, as quantum chemical calculations revealed (*vide infra*).

3.3.2. Emission in the crystalline state

As shown in Fig. 4, P-based chromophores **P1**–**P4** are also emissive in crystalline powder. Emission maxima ranged from 620 nm (**P4**) to 650 nm (**P1**) for measured quantum yield of a few percent (Table 1). In comparison, only **N2** and **N3**, bearing the weaker acceptors, are emissive

Table 1
Absorption maxima (λ_{max}^{abs}), molar absorptivity (ε), emission maximum (λ_{max}^{em}) for each dye in solution in acetone; Absorption and emission maxima (λ_{max}^{abs}), α_{AIE} and Stokes Shift ($\Delta\nu$) for nanoaggregates obtained in acetone/water mixture (10:90); Emission maximum (λ_{max}^{em}) and quantum yield (ϕ_F) in solid powder.

	Solution			Nanoaggregates				Solid	
	λ_{max}^{abs} (nm)	ε ($L.mol^{-1}cm^{-1}$)	λ_{max}^{em} (nm)	λ_{max}^{abs} (nm)	λ_{max}^{em} (nm)	α_{AIE} [a]	$\Delta\nu$ (cm^{-1})	λ_{max}^{em} (nm)	ϕ_F (%) [b]
P1	420	39 500	–	425	705	90	9350	650	1
P2	365	34 100	–	370	630	170	11 150	635	5
P3	370	29 000	–	380	625	50	10 300	655	4
P4	400	53 700	–	405	635	35	8950	620	7
N1	540	52 100	745	535	750	8	5350	–	–
N2	465	42 300	670	470	665	10	6250	635	34
N3	465	41 000	656	485	655	7	5350	645	9
N4	480	35 300	689	490	700	0.5	6100	–	–

[a] Defined as the fluorescence intensity ratio between acetone/water mixture (10/90) and pure acetone solution.

[b] Measured using a calibrated integrating sphere.

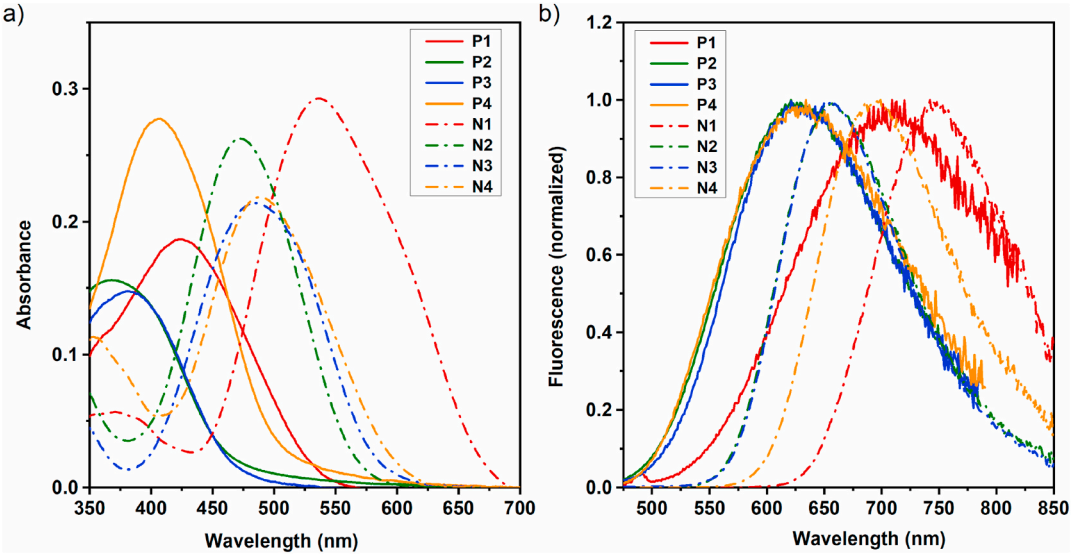

Fig. 3. a) Absorption and b) normalized emission spectra of dyes aggregates obtained in a 10:90 acetone/water mixture (10 μM)). The phosphorus based dyes **P1**–**P4** are represented using plain lines and the nitrogen based dyes **N1**–**N4** with dotted lines. λ_{exc} = 410 nm for P-dyes and λ_{exc} = 490 nm, for N-dyes except for **N1**, λ_{exc} = 540 nm.

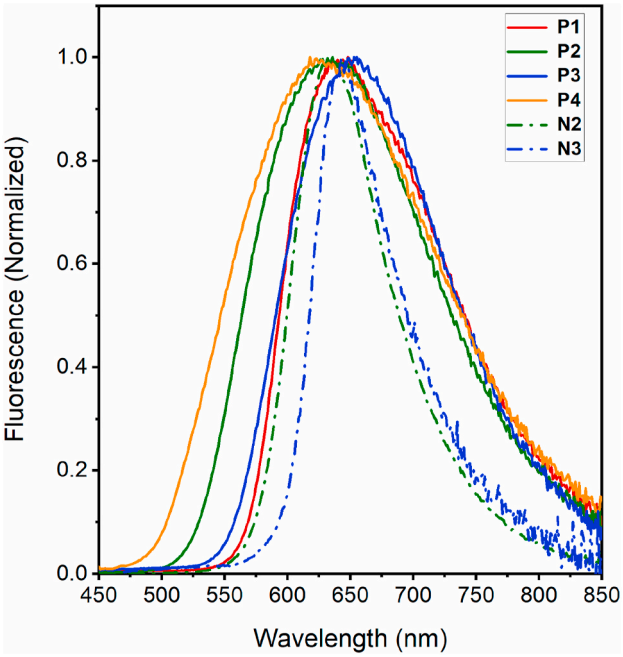

Fig. 4. Crystal state fluorescence spectra of dyes **P1**–**P4** (plain lines) and **N2**–**N3** (dotted lines). λ_{exc} = 390 or 400 nm for all dyes.

in crystalline powder, with quantum yields of 34% at 635 nm and 8% at 645 nm, respectively[51,52]. Here again, the hypsochromic shift observed between P-based dyes and their N-analogues is small.

3.4. Theoretical studies and comparison with crystal structures

To rationalize the optical properties observed, quantum chemical calculations were performed. A benchmark of exchange correlation functionals on the calculation of the S_0–S_1 transition energies compared to experimental values identifies M062X as the best functional for our study (Table SI 2). This functional was used in the rest of the study.

3.4.1. Structural variations between the ground- and the first excited-state

For the P-dyes **P1**–**P3**, considerable structural variations can be observed between the optimized structures of the ground state and first excited state in acetone, especially around the P-center. In the ground state, the P-centers adopt a trigonal pyramidal geometry, with an average height (h) of 0.79 Å for the pyramidal structure. Upon excitation, in the first excited state, the planarity of the compounds increases characterized by a decrease of the pyramid height of 0.20 Å on average. This increase of the planarity of the phosphorus donor and the conjugation of the π system is not observed for the **P4** compound which maintains the pyramidal geometry of its ground state (Table 2). Interestingly, this order of geometry reorganization according to the electron acceptor (0.00 for **P4**, 0.13 for **P1** and 0.22 for both **P2** and **P3**) perfectly matches with the order of Stokes shift values obtained experimentally (**P4** < **P1** < **P3** ≈ **P2**) and the fact that **P4** is the only P-dye fluorescent in (apolar) solution.

By contrast, for the N-dyes **N1**–**N4**, the geometry around the N donor atom is trigonal planar, both in the ground states and in the first excited states, with an average height of 0.01 Å. The comparison between the ground states and excited states of **P1** and **N1** is given in Fig. 5a.

3.4.2. Electronic density variations

The electronic density variations were also calculated and are represented in Fig. 5b for **N1** and **P1** and in SI for the other dyes. The red (blue) area represents a decrease (respectively enhancement) of the electronic density during the transition. In both N-dyes and P-dyes, the

Table 2
Heights for the pyramidal structure of the different compounds from DRX experiments (h^{RX}) or optimized structures of both ground and excited states from DFT/M062X calculations (respectively h^{DFT}_{GS} and h^{DFT}_{ES}).

	h^{RX}_{GS} (Å)	h^{DFT}_{GS} (Å)	h^{DFT}_{ES} (Å)
N1	–	0.01	0.00
N2	0.07	0.01	0.00
N3	0.05	0.02	0.01
N4	0.06	0.01	0.01
P1	0.82	0.79	0.66
P2	–	0.79	0.57
P3	–	0.80	0.57
P4	–	0.79	0.78

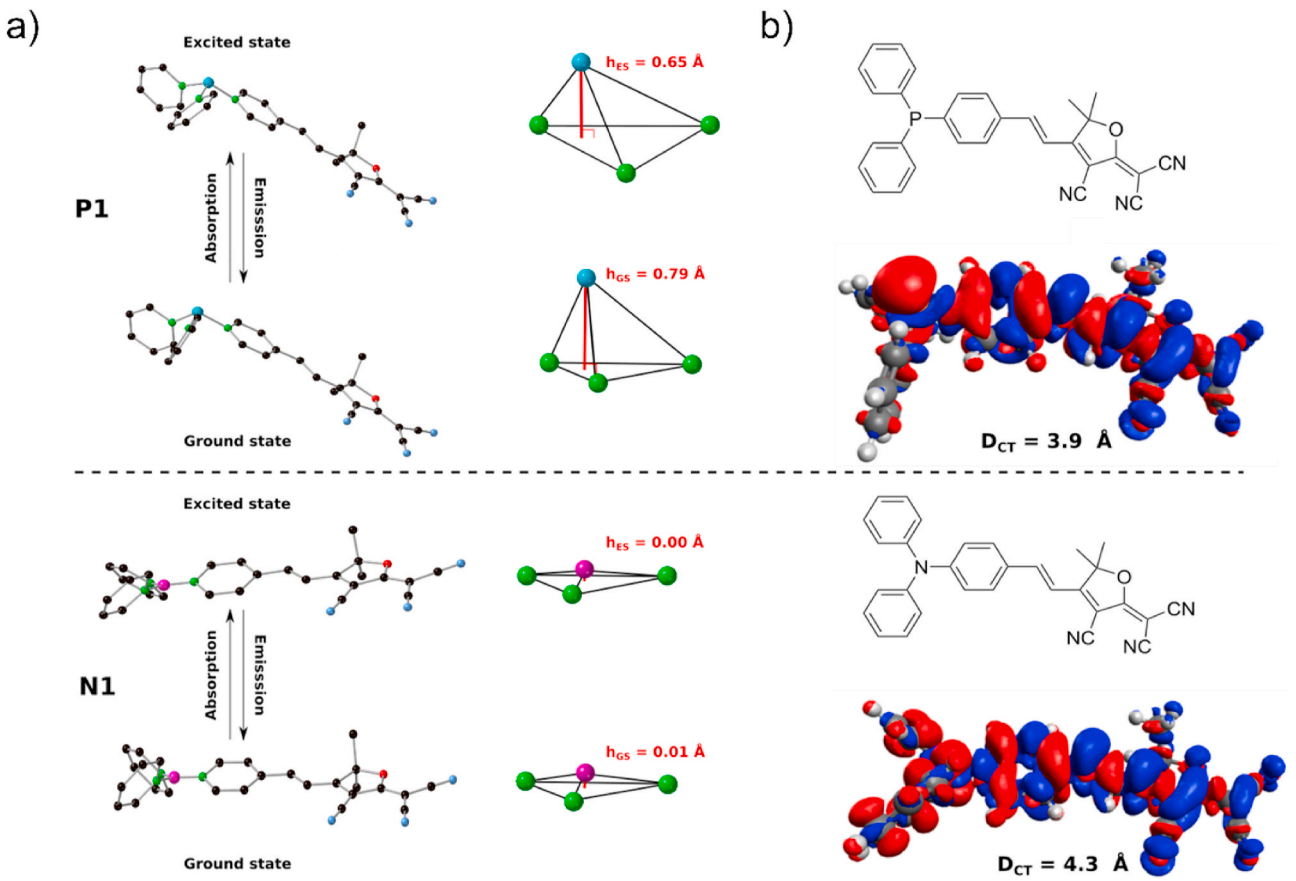

Fig. 5. a) Structural variations between the optimized structures of the ground state and the first excited state in acetone for **P1** (top) and **N1** (bottom) compounds. The optimized structures of both the ground and the excited states are shown on the left, while the pyramidal geometry around the P or N center is shown on the right. P and N-centers are represented in cyan and pink respectively, connected carbon atoms in green. b) Electronic density variations of **P1** (top) and **N1** (bottom) compounds. Red (blue) area represents a decrease (respectively enhancement) of the electronic density during the transition.

electronic density of the donor is depleted and that of the acceptor is enriched, which is consistent with the character of the strong charge transfer. However, the depletion of the donor side is quite different depending on the donor atom. In the case of the $(C_6H_5)_2P$- group, the charge transfer mainly originates from the lone pair of the phosphorus atom, highly localized on the upper side of the chromophore plane as shown in Fig. 5b. In the case of a $(C_6H_5)_2N$- donor, there is a stronger contribution of the orbitals of the phenyls rings and the lone pair is localized on both sides of the chromophore plane. Quantitatively, we estimated the strength of the charge transfer associated to the force transition by computing the D_{CT} index (Table SI 4), a parameter defining the spatial extent associated to the transition as well as the associated fraction of electron transferred[63]. From P- to N-dyes, the average D_{CT} increases by around 10%, from 4 Å to 4.4 Å, consistent with the stronger charge transfer within the amine dyes, as well as the implication of the orbitals of the phenyls.

3.4.3. *Comparison with X-ray crystal structures*

To probe the phenomenon more deeply, we studied the crystalline structures. Crystals suitable for X-ray diffraction analysis were obtained for **P1**, by slow diffusion of ethanol in chloroform. We previously reported the crystal structures of N-dyes **N2**[51], **N3** [52] and **N4** [50]. Unfortunately, all attempts to obtain crystals for **N1** and other P-dyes **P2**–**P4** only produced thin needles, unsuitable for X-ray diffraction. So, despite the acceptor difference, we chose to compare the solid-state structures of **P1** and **N4**, selected as a model of N-dyes (Fig. 6). The **N4** π system is quasi-planar, with only a small 10° angle between the acceptor and donor mean planes. In agreement with the calculations, the triphenylamino-moiety adopts a trigonal planar configuration, with a pyramid height of 0.06 Å (Fig. 6b, Fig. SI 14). Note that **N2** and **N3** show very similar planarity in their crystal structures (Figure SI-11 to SI-13). The **P1** π system is very similar to that of **N4**, with a small 12° angle between the acceptor and donor mean planes. On the other hand, Fig. 6 clearly shows the pyramidal configuration of phosphorus in **P1**. The measured pyramid height is 0.82 Å (Fig. 6a, Fig. SI 15), very close to the calculated value (0.79 Å) obtained by optimization of the ground state structure in acetone. Those geometry differences have consequences for the position of the lone pair, perpendicular to the π system for N-dyes and tilted to the back and to the side for P-dyes, thus, on the conjugation of the donor with the rest of the chromophore. All computationally obtained pyramid heights are given in Table 2, along with available DRX data. Finally, for both chromophores, neighbors are arranged in a dimeric head-to-tail configuration with an intermolecular distance of 3.2 Å for **N4** and 3.1 Å for **P1** (Fig. SI 16). Despite the enhanced steric hindrance of the out-of-plane phenyls of **P1** compared to **N4**, neighboring dyes are actually closer in the crystal arrangement of compound **P1**. On a larger scale, the herringbone arrangement of **P1** dyes, as viewed down the crystallographic *a* axis (Fig. SI 17), is usually considered as beneficial for solid state fluorescence.

4. Conclusion

The synthesis of four novel dyes based on the diphenylphosphino donor-group enabled us to study their optical properties in solution and in the solid state and compare them with the diphenylamino-analogues. Despite being quenched in solution, probably due to the intramolecular planarization movement of the phosphine donor, they light up in solid state (amorphous aggregates or crystalline powder) as typical AIE was

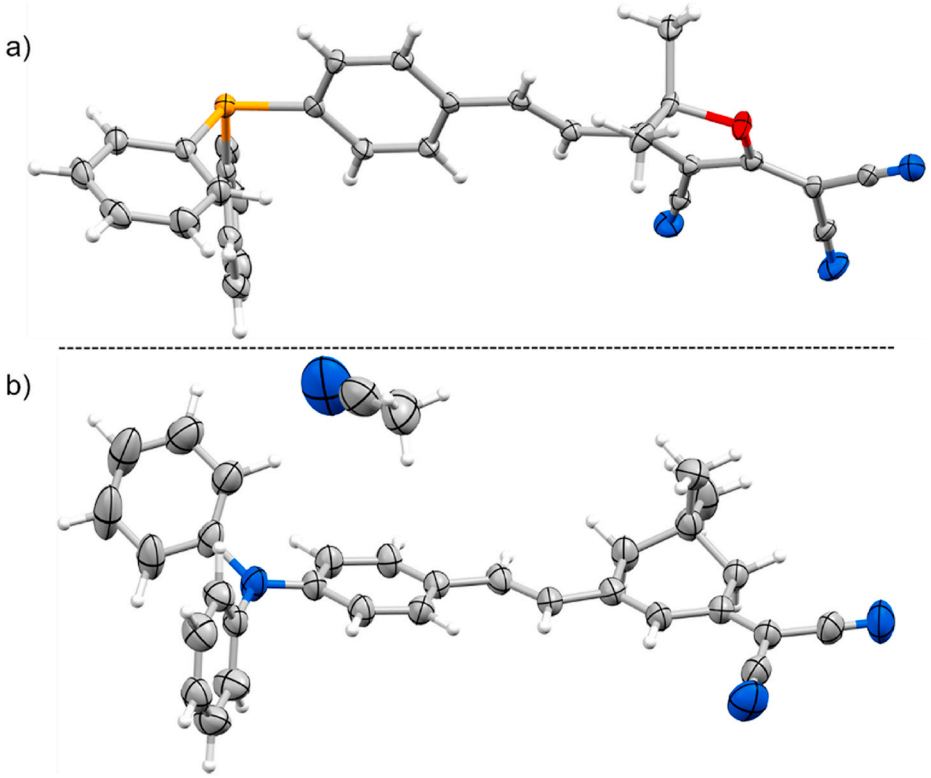

Fig. 6. Comparative views of the X-ray crystal structures of a) **P1** and b) **N4**, showing the pyramidal configuration of the phosphorus and the trigonal planar configuration of the nitrogen atom (ORTEP views with 50% probability displacement ellipsoids. H atoms are omitted for clarity. Compound **N4** crystallized with an acetonitrile molecule).

demonstrated by nanoprecipitation procedure involving a solvent shifting process. Phosphine aggregates showed higher fluorescence turn-on coefficients upon aggregation (170-fold increase emission for **P2**) than their amine analogues, but above all much larger Stokes shift (10 000 cm^{-1} on average), that can be attributed to large conformational changes around the P-atom between the ground state and the first excited state. In fine, we believe that the diphenylphosphino-can be an interesting donor group for the design of large Stokes shift fluorophores and could be used to control intramolecular packing in the solid-state, or could even be used in molecular machines as they are capable of producing small but reproducible planarity change upon light absorption.

Author contribution statement

Maxime Rémond: Experimentation, Methodology, Writing- Original draft preparation. **Pauline Colinet**: Calculation, Writing- Original draft preparation. **Erwann Jeanneau**: Crystallography. **Tanguy Le Bahers**: Supervision, Methodology, Calculation. **Chantal Andraud**: Supervision, Methodology, Validation. ***Yann Bretonnière*:** Supervision, Experimentation, Methodology, Writing- Original draft preparation, Writing- Reviewing and Editing.

Declaration of competing interest

The authors declare that they have no known competing financial interests or personal relationships that could have appeared to influence the work reported in this paper.

Appendix A. Supplementary data

Supplementary data to this article can be found online at https://doi.org/10.1016/j.dyepig.2021.109485.

References

[1] Li D, Zhang H, Wang Y. Four-coordinate Organoboron compounds for organic light-emitting Diodes (OLEDs). Chem Soc Rev 2013;42(21):8416–33. https://doi.org/10.1039/c3cs60170f.
[2] Mellerup SK, Wang S. Boron-based Stimuli responsive materials. Chem Soc Rev 2019;48(13):3537–49. https://doi.org/10.1039/c9cs00153k.
[3] Hirai M, Tanaka N, Sakai M, Yamaguchi S. Structurally constrained boron-, nitrogen-, Silicon-, and phosphorus-centered polycyclic π-conjugated systems. Chem Rev 2019;119(14):8291–331. https://doi.org/10.1021/acs.chemrev.8b00637.
[4] Zhao Q, Wang J, Freeman JL, Murphy-Jolly M, Wright AM, Scardino DJ, Hammer NI, Lawson CM, Gray GM. Syntheses, and optical, fluorescence, and nonlinear optical characterization of phosphine-substituted terthiophenes. Inorg Chem 2011;50(5):2015–27. https://doi.org/10.1021/ic101624y.
[5] Zhao Q, Freeman JL, Wang J, Zhang Y, Hamilton TP, Lawson CM, Gray GM. Syntheses, X-ray crystal structures, and optical, fluorescence, and nonlinear optical characterizations of diphenylphosphino-substituted Bithiophenes. Inorg Chem 2012;51(4):2016–30. https://doi.org/10.1021/ic201309k.
[6] Freeman JL, Zhao Q, Zhang Y, Wang J, Lawson CM, Gray GM. Synthesis, linear and nonlinear optical properties of phosphonato-substituted Bithiophenes derived from 2,2′-biphenol. Dalton Trans 2013;42(39):14281–97. https://doi.org/10.1039/c3dt51499d.
[7] Allen DW, Mifflin JP, Skabara PJ. Synthesis and solvatochromism of some dipolar aryl-phosphonium and -phosphine oxide systems. J Organomet Chem 2000;601(2):293–8. https://doi.org/10.1016/S0022-328X(00)00085-1.
[8] Lambert C, Gaschler W, Nöll G, Weber M, Schmälzlin E, Bräuchle C, Meerholz K. Cationic π-electron systems with High quadratic hyperpolarisability. J Chem Soc, Perkin Trans 2001;2(6):964–74. https://doi.org/10.1039/b009664b.
[9] Belyaev A, Cheng Y-H, Liu Z-Y, Karttunen AJ, Chou P-T, Koshevoy IO. A facile molecular machine: optically triggered counterion migration by charge transfer of linear donor-π-acceptor phosphonium fluorophores. Angew Chem Int Ed 2019;58(38):13456–65. https://doi.org/10.1002/anie.201906929.
[10] Alain-Rizzo V, Drouin-Kucma D, Rouxel C, Samb I, Bell J, Toullec PY, Michelet V, Leray I, Blanchard-Desce M. Synthesis, photophysical, and two-photon absorption properties of elongated Phosphane oxide and sulfide derivatives. Chem Asian J 2011;6(4):1080–91. https://doi.org/10.1002/asia.201000681.
[11] Bell J, Samb I, Toullec PY, Michelet V, Leray I. Synthesis and complexing properties of molecular probes linked with fluorescent Phosphane oxide derivatives. J Photochem Photobiol, A 2016;318:25–32. https://doi.org/10.1016/j.jphotochem.2015.11.017.
[12] Ha-Thi M-H, Souchon V, Hamdi A, Métivier R, Alain V, Nakatani K, Lacroix PG, Genêt J-P, Michelet V, Leray I. Synthesis of novel rod-shaped and star-shaped

fluorescent Phosphane oxides—nonlinear optical properties and photophysical properties. Chem Eur J 2006;12(35):9056–65. https://doi.org/10.1002/chem.200600464.
[13] Lambert C, Schmälzlin E, Meerholz K, Bräuchle C. Synthesis and nonlinear optical properties of three-dimensional phosphonium ion chromophores. Chem Eur J 1998;4(3):512–21.
[14] Baumgartner T, Réau R. Organophosphorus π-conjugated materials. Chem Rev 2006;106(11):4681–727. https://doi.org/10.1021/cr040179m.
[15] Crassous J, Réau R. π-Conjugated phosphole derivatives: synthesis, optoelectronic functions and coordination Chemistry. Dalton Trans 2008;48:6865–76. https://doi.org/10.1039/b810976a.
[16] Bouit P-A, Escande A, Szűcs R, Szieberth D, Lescop C, Nyulászi L, Hissler M, Réau R. Dibenzophosphapentaphenes: exploiting P Chemistry for Gap fine-tuning and coordination-driven assembly of planar polycyclic aromatic Hydrocarbons. J Am Chem Soc 2012;134(15):6524–7. https://doi.org/10.1021/ja300171y.
[17] Stolar M, Baumgartner T. Phosphorus-containing materials for organic electronics. Chem Asian J 2014;9(5):1212–25. https://doi.org/10.1002/asia.201301670.
[18] Baumgartner T. Insights on the design and electron-acceptor properties of conjugated Organophosphorus materials. Acc Chem Res 2014;47(5):1613–22. https://doi.org/10.1021/ar500084b.
[19] Duffy MP, Delaunay W, Bouit PA, Hissler M. π-Conjugated phospholes and their incorporation into Devices: Components with a great deal of potential. Chem Soc Rev 2016;45(19):5296–310. https://doi.org/10.1039/c6cs00257a.
[20] Zhou Y, Yang S, Li J, He G, Duan Z, Mathey F. Phosphorus and silicon-bridged stilbenes: synthesis and optoelectronic properties. Dalton Trans 2016;45(45):18308–12. https://doi.org/10.1039/c6dt03489f.
[21] Shameem MA, Orthaber A. Organophosphorus compounds in organic electronics. Chem Eur J 2016;22(31):10718–35. https://doi.org/10.1002/chem.201600005.
[22] Wang C, Fukazawa A, Tanabe Y, Inai N, Yokogawa D, Yamaguchi S. Water-soluble phospholo[3,2-b]phosphole-P,P′-Dioxide-Based fluorescent dyes with High photostability. Chem Asian J 2018;13(12):1616–24. https://doi.org/10.1002/asia.201800533.
[23] Higashino T, Ishida K, Satoh T, Matano Y, Imahori H. Phosphole–thiophene hybrid: a dual Role of dithieno[3,4-b:3′,4′-d]phosphole as electron acceptor and electron donor. J Org Chem 2018;83(6):3397–402. https://doi.org/10.1021/acs.joc.8b00030.
[24] Fukazawa A, Yamada H, Yamaguchi S. Phosphonium- and borate-bridged zwitterionic ladder stilbene and its extended analogues. Angew Chem Int Ed 2008;47(30):5582–5. https://doi.org/10.1002/anie.200801834.
[25] Chai X, Cui X, Wang B, Yang F, Cai Y, Wu Q, Wang T. Near-infrared phosphorus-substituted rhodamine with emission wavelength above 700nm for bioimaging. Chem Eur J 2015;21(47):16754–8. https://doi.org/10.1002/chem.201502921.
[26] Jiang X-D, Zhao J, Xi D, Yu H, Guan J, Li S, Sun C-L, Xiao L-J. A New water-soluble phosphorus-dipyrromethene and phosphorus-azadipyrromethene dye: PODIPY/aza-PODIPY. Chem Eur J 2015;21(16):6079–82. https://doi.org/10.1002/chem.201406535.
[27] Zhou X, Lai R, Beck JR, Li H, Stains CI. Nebraska red: a phosphinate-based near-infrared fluorophore Scaffold for chemical Biology applications. Chem Commun 2016;52(83):12290–3. https://doi.org/10.1039/c6cc05717a.
[28] Fukazawa A, Suda S, Taki M, Yamaguchi E, Grzybowski M, Sato Y, Higashiyama T, Yamaguchi S. Phospha-fluorescein: a red-emissive Fluorescein analogue with High photobleaching resistance. Chem Commun 2016;52(6):1120–3. https://doi.org/10.1039/c5cc09345g.
[29] Fukazawa A, Usuba J, Adler RA, Yamaguchi S. Synthesis of seminaphtho-phospha-fluorescein dyes based on the consecutive arylation of aryldichlorophosphines. Chem Commun 2017;53(61):8565–8. https://doi.org/10.1039/c7cc04323f.
[30] Grzybowski M, Taki M, Yamaguchi S. Selective conversion of P=O-bridged rhodamines into P=O-rhodols: solvatochromic near-infrared fluorophores. Chem Eur J 2017;23(53):13028–32. https://doi.org/10.1002/chem.201703456.
[31] Hashimoto N, Umano R, Ochi Y, Shimahara K, Nakamura J, Mori S, Ohta H, Watanabe Y, Hayashi M. Synthesis and photophysical properties of λ^5-phosphinines as a tunable fluorophore. J Am Chem Soc 2018;140(6):2046–9. https://doi.org/10.1021/jacs.7b13018.
[32] Grzybowski M, Taki M, Senda K, Sato Y, Ariyoshi T, Okada Y, Kawakami R, Imamura T, Yamaguchi S. A highly photostable near-infrared labeling agent based on a phospha-rhodamine for long-term and Deep imaging. Angew Chem Int Ed 2018;57(32):10137–41. https://doi.org/10.1002/anie.201804731.
[33] Ogasawara H, Grzybowski M, Hosokawa R, Sato Y, Taki M, Yamaguchi S. A far-red fluorescent probe based on a phospha-fluorescein Scaffold for cytosolic Calcium imaging. Chem Commun 2018;54(3):299–302. https://doi.org/10.1039/c7cc07344e.
[34] Wang L, Du W, Hu Z, Uvdal K, Li L, Huang W. Hybrid rhodamine fluorophores in the visible/NIR region for biological imaging. Angew Chem Int Ed 2019;58(40):14026–43. https://doi.org/10.1002/anie.201901061.
[35] Belyaev A, Chen Y-T, Liu Z-Y, Hindenberg P, Wu C-H, Chou P-T, Romero-Nieto C, Koshevoy IO. Intramolecular phosphacyclization: polyaromatic phosphonium P-heterocycles with wide-tuning optical properties. Chem Eur J 2019;25(25):6332–41. https://doi.org/10.1002/chem.201900136.
[36] Bard JP, Bates HJ, Deng C-L, Zakharov LN, Johnson DW, Haley MM. Amplification of the quantum yields of 2-λ^5-Phosphaquinolin-2-ones through phosphorus center modification. J Org Chem 2020;85(1):85–91. https://doi.org/10.1021/acs.joc.9b02132.
[37] Sauer M, Nasufovic V, Arndt H-D, Vilotijevic I. Robust synthesis of NIR-emissive P-rhodamine fluorophores. Org Biomol Chem 2020;18(8):1567–71. https://doi.org/10.1039/d0ob00189a.
[38] Davies LH, Harrington RW, Clegg W, Higham LJ. $^{B}R_2BodPR_2$: highly fluorescent Alternatives to PPh_3 and $PhPCy_2$. Dalton Trans 2014;43(36):13485–99. https://doi.org/10.1039/c4dt00704b.
[39] Davies LH, Stewart B, Harrington RW, Clegg W, Higham LJ. Air-stable, highly fluorescent primary phosphanes. Angew Chem Int Ed 2012;51(20):4921–4. https://doi.org/10.1002/anie.201108416.
[40] Onoda M, Tokuyama H, Uchiyama S, Mawatari K-i, Santa T, Kaneko K, Imai K, Nakagomi K. Fluorescence enhancement by Hydroperoxides based on a change in the intramolecular charge transfer character of benzofurazan. Chem Commun 2005;14:1848–50. https://doi.org/10.1039/b500419e.
[41] Tirla A, Rivera-Fuentes P. Development of a photoactivatable phosphine probe for induction of intracellular reductive stress with single-cell precision. Angew Chem Int Ed 2016;55(47):14709–12. https://doi.org/10.1002/anie.201608779.
[42] Hatakeyama T, Hashimoto S, Nakamura M. Tandem phospha-Friedel−Crafts reaction toward curved π-conjugated frameworks with a phosphorus ring junction. Org Lett 2011;13(8):2130–3. https://doi.org/10.1021/ol200571s.
[43] Smith JN, Hook JM, Lucas NT. Superphenylphosphines: nanographene-based Ligands that control coordination geometry and drive supramolecular assembly. J Am Chem Soc 2018;140(3):1131–41. https://doi.org/10.1021/jacs.7b12251.
[44] Madrigal LG, Spangler CW. The synthesis of Diphenylpolenes and PPV-oligomers incorporating diphenylphosphino donor groups. MRS Proceedings 1999;561:75. https://doi.org/10.1557/PROC-561-75.
[45] Madrigal L, Kuhl K, Spangler C. Photonic properties of Dendrons and Dendrimers incorporating bis-(Diphenylphosphino)Diphenylpolyenes. MRS Proceedings 2011;598. https://doi.org/10.1557/PROC-598-BB8.9. BB8.9.
[46] Madrigal L, Spangler C. Diphenylphosphino-substituted Diphenylpolyenes for applications in nonlinear Optics. Proc SPIE 1999;3796. https://doi.org/10.1117/12.368275.
[47] Yuan Z, Taylor NJ, Marder TB, Williams ID, Kurtz SK, Cheng L-T. Three coordinate phosphorus and boron as π-donor and π-acceptor Moieties respectively, in conjugated organic molecules for nonlinear Optics: crystal and molecular structures of E-ph–CH=CH–B(mes)$_2$, E-4-MeO–C_6H_4–CH=CH-B(mes)$_2$, and E-ph_2P–CH=CH–B(mes)$_2$ [mes = 2,4,6-$me_3C_6H_2$]. J Chem Soc, Chem Commun 1990;(21):1489–92. https://doi.org/10.1039/c39900001489.
[48] Agou T, Kobayashi J, Kawashima T. Dibenzophosphaborin: A hetero-π-conjugated molecule with fluorescent properties based on intramolecular charge transfer between phosphorus and boron atoms. Org Lett 2005;7(20):4373–6. https://doi.org/10.1021/ol051537q.
[49] He X, Borau-Garcia J, Woo AYY, Trudel S, Baumgartner T. Dithieno[3,2-c:2′,3′-e]-2,7-diketophosphepin: a unique building block for multifunctional π-conjugated materials. J Am Chem Soc 2013;135(3):1137–47. https://doi.org/10.1021/ja310680x.
[50] Massin J, Dayoub W, Mulatier J-C, Aronica C, Bretonnière Y, Andraud C. Near-infrared solid-state Emitters based on Isophorone: synthesis, crystal structure and spectroscopic properties. Chem Mater 2011;23(3):862–73. https://doi.org/10.1021/cm102165r.
[51] Yan X, Remond M, Zheng Z, Hoibian E, Soulage C, Chambert S, Andraud C, Van der Sanden B, Ganachaud F, Bretonnière Y, Bernard J. General and scalable approach to Bright, stable, and functional AIE fluorogen colloidal Nanocrystals for in Vivo imaging. ACS Appl Matet Interfaces 2018;10(30):25154–65. https://doi.org/10.1021/acsami.8b07859.
[52] Redon S, Eucat G, Ipuy M, Jeanneau E, Gautier-Luneau I, Ibanez A, Andraud C, Bretonnière Y. Tuning the solid-state emission of small push-pull dipolar dyes to the far-red through variation of the electron-acceptor group. Dyes Pigments 2018;156:116–32. https://doi.org/10.1016/j.dyepig.2018.03.049.
[53] Ipuy M, Liao Y-Y, Jeanneau E, Baldeck PL, Bretonnière Y, Andraud C. Solid state red biphotonic excited emission from small dipolar fluorophores. J Mater Chem C 2016;4(4):766–79. https://doi.org/10.1039/c5tc03465e.
[54] Nishi H, Namari T, Kobatake S. Photochromic polymers bearing various diarylethene chromophores as the pendant: synthesis, optical properties, and multicolor photochromism. J Mater Chem 2011;21(43):17249–58. https://doi.org/10.1039/c1jm12707a.
[55] Mei J, Wang J, Qin A, Zhao H, Yuan W, Zhao Z, Sung HHY, Deng C, Zhang S, Williams ID, Sun JZ, Tang BZ. Construction of soft porous crystal with silole derivative: strategy of framework design, multiple structural transformability and mechanofluorochromism. J Mater Chem 2012;22(10):4290–8. https://doi.org/10.1039/c1jm12673c.
[56] Xu G, Lei H, Zhou G, Zhang C, Xie L, Zhang W, Cao R. Boosting hydrogen evolution by using covalent frameworks of fluorinated cobalt porphyrins supported on carbon nanotubes. Chem Commun 2019;55(84):12647–50. https://doi.org/10.1039/C9CC06916J.
[57] Hon Y-S, Lee C-F, Chen R-J, Szu P-H. Acetonyltriphenylphosphonium bromide and its polymer-supported analogues as catalysts in protection and deprotection of alcohols as alkyl vinyl ethers. Tetrahedron 2001;57(28):5991–6001. https://doi.org/10.1016/S0040-4020(01)00558-0.
[58] Xia X, Toy PH. Polyethyleneimine-supported triphenylphosphine and its use as a highly loaded bifunctional polymeric reagent in chromatography-free one-pot Wittig reactions. Synlett 2015;26(12):1737–43. https://doi.org/10.1055/s-0034-1380810.
[59] García-Álvarez R, Díez J, Crochet P, Cadierno V. Arene−Ruthenium(II) Complexes containing Amino−Phosphine Ligands as catalysts for nitrile hydration reactions. Organometallics 2010;29(17):3955–65. https://doi.org/10.1021/om1006227.
[60] Frisch MJ, Trucks GW, Schlegel HB, Scuseria GE, Robb MA, Cheeseman JR, Scalmani G, Barone V, Petersson GA, Nakatsuji H, Li X, Caricato M, Marenich AV, Bloino J, Janesko BG, Gomperts R, Mennucci B, Hratchian HP, Ortiz JV, Izmaylov AF, Sonnenberg JL, Williams, Ding F, Lipparini F, Egidi F, Goings J, Peng B,

Petrone A, Henderson T, Ranasinghe D, Zakrzewski VG, Gao J, Rega N, Zheng G, Liang W, Hada M, Ehara M, Toyota K, Fukuda R, Hasegawa J, Ishida M, Nakajima T, Honda Y, Kitao O, Nakai H, Vreven T, Throssell K, Montgomery Jr JA, Peralta JE, Ogliaro F, Bearpark MJ, Heyd JJ, Brothers EN, Kudin KN, Staroverov VN, Keith TA, Kobayashi R, Normand J, Raghavachari K, Rendell AP, Burant JC, Iyengar SS, Tomasi J, Cossi M, Millam JM, Klene M, Adamo C, Cammi R, Ochterski JW, Martin RL, Morokuma K, Farkas O, Foresman JB, Fox DJ. Gaussian 16 Rev. C.01. Wallingford, CT2016.

[61] Zhao Y, Truhlar DG. The M06 suite of density functionals for main group Thermochemistry, thermochemical Kinetics, noncovalent interactions, excited states, and transition elements: two New functionals and systematic testing of four M06-class functionals and 12 other functionals. Theor Chem Acc 2008;120(1): 215–41. https://doi.org/10.1007/s00214-007-0310-x.

[62] Cossi M, Rega N, Scalmani G, Barone V. Energies, structures, and electronic properties of molecules in solution with the C-PCM solvation model. J Comput Chem 2003;24(6):669–81. https://doi.org/10.1002/jcc.10189.

[63] Le Bahers T, Adamo C, Ciofini I. A qualitative index of spatial extent in charge-transfer excitations. J Chem Theor Comput 2011;7(8):2498–506. https://doi.org/10.1021/ct200308m.

[64] Kwong FY, Lai CW, Yu M, Chan KS. Application of palladium-catalyzed Pd–aryl/P–aryl exchanges: preparation of functionalized aryl phosphines by phosphination of aryl bromides using triarylphosphines. Tetrahedron 2004;60(26):5635–45. https://doi.org/10.1016/j.tet.2004.04.085.